Journal Pre-proof

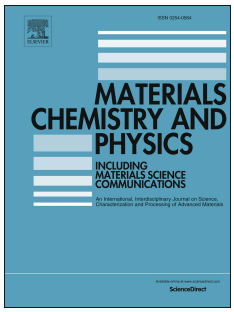

TiO_2 nanorods doped with g-C_3N_4 – Polyethylene composite coating for self-cleaning applications

Paula Osorio-Vargas, Daniel Pais-Ospina, Diego A. Marin-Silva, Adriana Pinotti, Laura Damonte, Antonela Cánneva, Jorge A. Donadelli, Luiz Pereira da Costa, Luis R. Pizzio, Cecilia C. Torres, Cristian H. Campos, Julián A. Rengifo-Herrera

PII: S0254-0584(22)00662-9

DOI: https://doi.org/10.1016/j.matchemphys.2022.126356

Reference: MAC 126356

To appear in: *Materials Chemistry and Physics*

Received Date: 28 December 2021

Revised Date: 28 April 2022

Accepted Date: 3 June 2022

Please cite this article as: P. Osorio-Vargas, D. Pais-Ospina, D.A. Marin-Silva, A. Pinotti, L. Damonte, A. Cánneva, J.A. Donadelli, L. Pereira da Costa, L.R. Pizzio, C.C. Torres, C.H. Campos, Juliá.A. Rengifo-Herrera, TiO_2 nanorods doped with g-C_3N_4 – Polyethylene composite coating for self-cleaning applications, *Materials Chemistry and Physics* (2022), doi: https://doi.org/10.1016/j.matchemphys.2022.126356.

Credit Authors Statement

Paula Osorio-Vargas: Conceptualization, Methodology, Investigation, Formal Analysis, Visualization, Supervision, Project Administration, and Funding Acquisition. **Daniel Pais-Ospina:** Investigation, and Data curation. **Diego A. Marín-Silva:** Data curation. **Adriana Pinotti:** Conceptualization, Methodology, Resources and Writing Review & Editing. **Laura Damonte:** Data curation. **Antonela Cánneva:** Data curation. **Jorge A. Donadelli:** Data curation. **Luiz Pereira Da Costa:** Data curation. **Luis R. Pizzio:** Conceptualization, Project Administration, and Funding Acquisition. **Cecilia C. Torres:** Methodology, and Resources. **Julián A. Rengifo-Herrera:** Conceptualization, Methodology, Supervision, Writing-original draft, Project Administration, and Funding Acquisition. **Cristian H. Campos:** Formal analysis, Supervision, Methodology, Data curation, and Writing Review & Editing.

TiO_2 nanorods doped with g-C_3N_4 – polyethylene composite coating for self-cleaning applications

Paula Osorio-Vargas[a,b], Daniel Pais-Ospina[c], Diego A. Marin-Silva[d], Adriana Pinotti[d,e], Laura Damonte[f], Antonela Cánneva[g], Jorge A. Donadelli[g], Luiz Pereira da Costa[h], Luis R. Pizzio[a], Cecilia C. Torres[i], Cristian H. Campos[j]*, and Julián A. Rengifo-Herrera[a]*

[a] Centro de Investigación y Desarrollo en Ciencias Aplicadas "Dr. J.J. Ronco" (CINDECA), Departamento de Química, Facultad de Ciencias Exactas, UNLP-CCT La Plata, CONICET, 47 No. 257, 1900 La Plata, Buenos Aires, Argentina

[b] Escuela de Ingeniería Química, Departamento de Ingeniería en Maderas, Universidad del Bío-Bío, Chile

[c] Grupo de investigación en Fotocatálisis y Estado sólido, Universidad Tecnológica de Pereira, Escuela de Química, Vereda la Julita, Pereira, Risaralda, 660003, Colombia

[d] Centro de Investigación y Desarrollo en Criotecnología de Alimentos (CIDCA), CONICET, La Plata, Facultad de Ciencias Exactas, UNLP, 47 y 116, 1900 La Plata, Argentina

[e] Facultad de Ingeniería, Universidad Nacional de La Plata, La Plata Argentina

[f] Instituto de Física La Plata (IFLP, CONICET – FCE UNLP) Diag. 113 e/ 63 y 64, (1900) La Plata, Buenos Aires (Argentina)

[g] CONICET, YPF TECNOLOGÍA S. A. Av. Del Petroleo s/n – (Entre 129 y 143), (1925) Berisso – Buenos Aires, Argentina

[h] Graduate Program in Science and Technology for Amazon Resources (PPGCTRA)-Institute of Exact Sciences and Technology (ICET/UFAM), Rua: Nossa Senhora do Rosario, 3863, Tiradentes, Itacoatiara-Amazonas, CEP.: 69103-128

[i] Departamento de Ciencias Químicas, Facultad de Ciencias Exactas, Universidad Andrés Bello, Sede Concepción, Autopista Concepción-Talcahuano 7100, Talcahuano, Chile

[j] Universidad de Concepción, Facultad de Ciencias Químicas, Departamento de Físico-Química, Edmundo Larenas 129. Concepción, Chile

Corresponding authors:

Cristian H. Campos. e-mail: ccampos@udec.cl

Julián A. Rengifo-Herrera. e-mail: julianregifo@quimica.unlp.edu.ar

Graphical Abstract

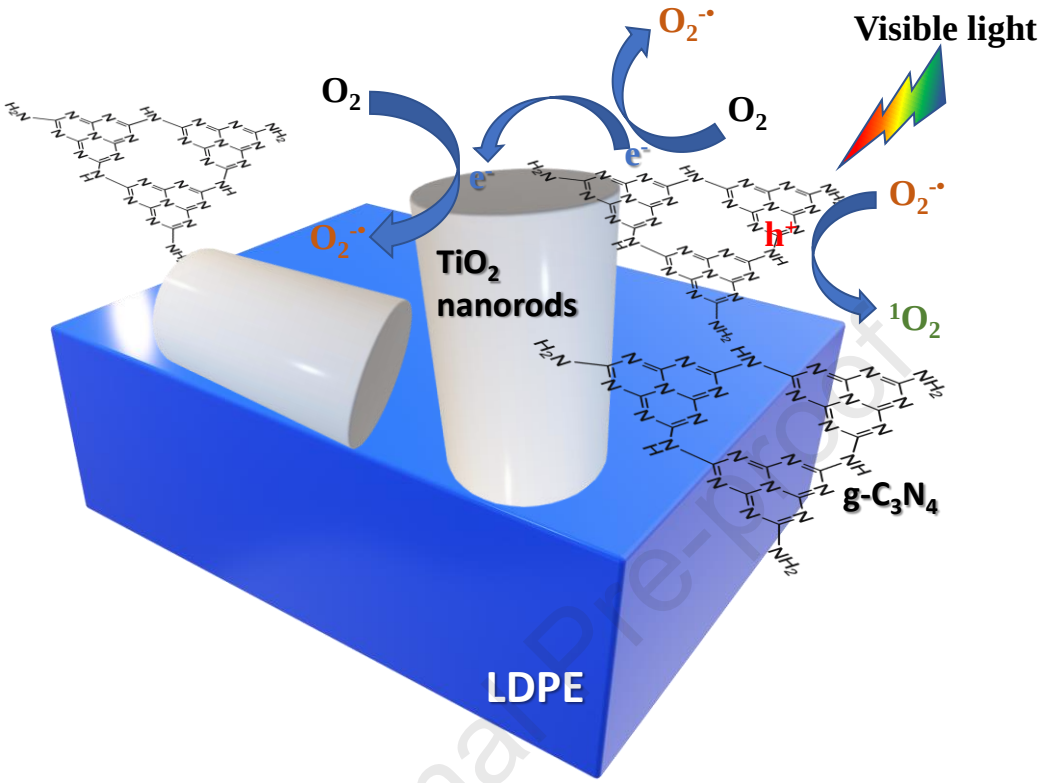

Abstract

Visible-light-absorbing graphitic carbon nitride–TiO_2 nanorod nanomaterials (g-C_3N_4@TiO_2NR) were successfully immobilized using a one-step UVA-induced photocatalytic procedure on commercially obtained flexible low-density polyethylene (LDPE) films. Self-cleaning properties were evaluated in solid–liquid and solid–gas phases using malachite green as a model molecule under UV-A and visible light irradiation. For comparison purpose, LDPE films containing P25 TiO_2 nanoparticles was prepared using the same synthetic strategy (P25/LDPE). Among the fabricated films, the g-C_3N_4@TiO_2NR/LDPE films exhibited the highest photocatalytic activity both in solid–liquid and solid–gas phases after 120 min of visible light irradiation (λ > 455 nm) removing efficiently malachite green stains probably due to the attack of photoinduced reactive oxygen species (ROS) such as singlet oxygen ($^1O_2$), hydroxyl radical ($^{\bullet}OH$) and superoxide anion radical ($O_2^{-\bullet}$). Furthermore, the g-C_3N_4@TiO_2NR/LDPE films retained their visible-light-photoinduced photocatalytic properties after four reuse cycles. The g-C_3N_4@TiO_2NR/LDPE films also exhibited significant visible-light-photoinduced hydrophilicity. The high visible-light-photoinduced photocatalytic capacity of g-C_3N_4@TiO_2NR/LDPE films was found to be related to the textural and electronic properties, superior visible-light absorption, and surface roughness of the films.

Keywords: TiO_2@g-C_3N_4 composites, visible-light-responsive materials, self-cleaning materials, photoinduced composites synthesis.

1. Introduction

Polymeric surfaces containing TiO_2 or visible-light-absorbing TiO_2 nanomaterials have been extensively applied as photo-induced self-cleaning materials under ultraviolet (UV), visible, or indoor light irradiation [1–6]. However, achieving a high photoconversion efficiency of reactive oxygen species (ROS) such as hydroxyl radicals ($^{\bullet}OH$), superoxide anion radical ($O_2^{-\bullet}$), hydrogen peroxide (H_2O_2) and singlet oxygen ($^1O_2$) is often hindered by slow electron diffusion through a random TiO_2 nanoparticle network and an enhanced electron–hole pair recombination rate. Several recent studies have reported [7–10] the use of nanostructured TiO_2 with enhancements in photocatalytic activity owing to (i) the reduction of recombination via its highly ordered architecture, (ii) its high specific surface area, and (iii) enhanced generation of $^{\bullet}OH$ radicals because of the presence of a significant number of surface –OH groups.

The improved photocatalytic performance of nanostructured TiO_2 owing to these properties can facilitate its application as a promising self-cleaning surface upon immobilization on a polymeric surface. TiO_2 is typically immobilized on polymeric materials through casting and extrusion methods, wherein TiO_2-based materials are embedded onto the polymer structure [4].

Metal oxide nanoparticles can also be immobilized on functionalized polymeric surfaces. The formation of oxygenated groups such as C=O, C–OH, and –COOH facilitates interactions between metal oxide nanoparticles and polymer surfaces. Plasma and vacuum ultraviolet pretreatments are frequently employed to achieve polymer surface functionalization; however, these techniques require the use of expensive equipment [1,11–13]. Mazille et al. [14] reported a novel strategy to immobilize TiO_2 nanoparticles onto polyvinyl fluoride films via a one-step photoinduced immobilization. Under UV irradiation, TiO_2 nanoparticles produce ROS such as $^{\bullet}OH$ radicals that attack the polymer surface to create –C=O and –COOH functional groups on the polymer surface. Using pH adjustment (which determines the surface charge of TiO_2 nanoparticles), the electrostatic interaction between TiO_2 and polymer surface was enhanced to facilitate immobilization of the semiconductor. Mena et al. [15] discussed the photocorrosion of polyethylene films in P25 TiO_2 suspensions in the presence of $FeCl_3$ under UV-A light irradiation for 15 h; P25 and FeO_x were subsequently immobilized via binding with surficial oxidative chelating sites.

These films exhibited significant activities for the deactivation of *Escherichia coli* cells under simulated sunlight irradiation. Alvear-Daza et al. [16] recently investigated the one-step photocatalytic immobilization of P25 nanoparticles onto low-density polyethylene (LDPE) films. LDPE was found to undergo surficial functionalization via an attack of photoinduced ROS such as •OH radicals, which resulted in P25 nanoparticle deposition. The photocatalytic immobilization was noted to depend on several variables, such as the amount of P25, initial pH of the suspension, and irradiation time.

TiO_2/g-C_3N_4 composites immobilized on glass, cotton cellulose and polytetrafluorethylene (PTFE) have been evaluated as self-cleaning surfaces (Table 1). Commercial (P25) and sol-gel synthesized TiO_2 nanoparticles were annealed in presence of melamine at temperatures oscillating between 400 and 500 °C to obtain TiO_2/g-C_3N_4 nanocomposites. Then, these nanomaterials were immobilized on glass (by spray-coating), PTFE membranes by plasma polymer functionalization and generating in situ on cotton fibers the TiO_2/g-C_3N_4 nanocomposites by hydrothermal treatment in a Teflon-covered stainless-steel autoclave heated at 120 °C for 4 h. These materials were then photocatalytically evaluated using the dyes methylene blue (MB) and methyl orange (MO) as pollutant and oxidizing NO_x under visible light irradiation (λ> 420 nm). It was also evaluated the wettability properties of glass-TiO_2/g-C_3N_4 materials obtaining a contact angle (CA) reduction after 3 min of sunlight irradiation. Photocatalytic activity of polymeric films evaluated with organic dyes as pollutants exhibited an encouraging dye degradation, however, photosensitized reactions induced by dye excited states were not discarded. On the other hand, no reports about nanostructured TiO_2 n as nanorods containing g-C_3N_4 immobilized on polymeric substrates as self-cleaning surfaces were not found in the literature.

Table 1. Immobilized TiO_2/g-C_3N_4 nanocomposites on several supports and their self-cleaning properties under visible light irradiation

Synthesis	Immobilization Support	Photocatalytic activity	Reference
P25 nanoparticles and melamine as g-C_3N_4 precursor annealed at 520 °C for 4 h	PTFE polymer (Polymer plasma functionalization)	Solid-liquid interface. Methylene blue (MB) dye solution as pollutant and irradiation at λ> 400 nm (Xe lamp)	[17]
Sol-gel method using tetrabutyl titanate (TBT)	Glass (spray coating)	Solid-gas interface. NO_x oxidation and contact angle	[18]

and melamine and Annealing at 550 °C for 3 h		measurement at at λ> 400 nm and sunlight irradiation	
Sol-gel method using TBT and melamine. Hydrothermal treatment at 120 °C for 4 h	Impregnation of nanocomposites on cotton cellulose fibers under hydrothermal conditions	Solid-liquid interface. Methyl orange (MO) dyesolution as pollutant and irradiation at λ> 420-620 nm (LED lamp)	[19]

The present study involved the preparation, characterization, and photocatalytic activity analysis of visible-light-absorbing g-C_3N_4@TiO_2 nanorod composites deposited on flexible LDPE films using a novel one-step method based on photocatalytic immobilization under UV irradiation. g-C_3N_4/TiO_2 nanocomposites [20–26] are known to facilitate visible light responses (E_{bg} = 2.69 eV) into these materials [27]. This new immobilization procedure exhibits the advantage to photocatalytically functionalize the polymer surface creating oxygenated carbon groups and, at the same time, achieve the g-C_3N_4@TiO_2 nanorod composites immobilization in one step due to interactions between the nanoparticles and the oxygenated functional groups without the use of plasma or UV pretreatment. To investigate the self-cleaning properties of the film surfaces, the photocatalytic activity was evaluated in solid–liquid and solid–gas interfaces using malachite green dye as a model pollutant under UV and visible light irradiation. The nanostructured materials and films were characterized using various techniques.

2. Material and methods

2.1 Materials

Titanium tetraisopropoxide (99%, Sigma-Aldrich), urea (99%, Sigma-Aldrich), malachite green oxalate (99%, Sigma-Aldrich), ethanol (absolute grade, Merck), P25 TiO_2 nanoparticles (Evonik), HCl (37%, Carlo Erba), NaOH (Merck), and HNO_3 (65%, Sigma-Aldrich) were employed in this study. LDPE films with a thickness of 0.1 mm were obtained from Longfellow (ET3112019). All chemicals were used as received.

2.2 *Synthesis and characterization of g-C_3N_4@TiO_2 nanorods (g-C_3N_4@TiO_2NR)*

Graphitic carbon nitride–TiO_2 nanorod (g-C_3N_4@TiO_2NR) composites were prepared using a two-step procedure. First, nanostructured TiO_2 was prepared using a previously reported hydrothermal method [28]. The Na-titanates obtained using this method were washed with HNO_3 (0.10 mol L^{-1}) to yield H-titanates, which were subsequently suspended in a urea solution in a H-titanate:urea ratio of 1:4. This ratio was selected to facilitate optimal visible light absorption and photocatalytic performance [29]. The suspension was dried at 80 °C overnight and annealed at 450 °C for 1 h to obtain g-C_3N_4@TiO_2-nanorod composites (g-C_3N_4@TiO_2NR).

The physical and chemical characterization of the g-C_3N_4@TiO_2NRs was performed using diffuse reflectance spectroscopy (DRS), powder X-ray diffraction (XRD), attenuated total reflectance–Fourier-transform infrared spectroscopy (ATR–FTIR), Z potential analysis, transmission electronic microscopy (TEM), N_2 adsorption–desorption, and X-ray photoelectron spectroscopy (XPS). All experimental details are provided in the supplementary material.

2.3 Synthesis and characterization of LDPE films containing g-C_3N_4@TiO_2 nanorods (g-C_3N_4@TiO_2NR/LDPE)

Commercially obtained LDPE films (9.0 cm × 4.0 cm) were placed in a 100 mL beaker containing Milli-Q water and ethanol for cleaning in an ultrasonic bath (for 5 min) prior to the photocatalytic immobilization. The films were dried at temperatures oscillating between 20-25 °C for 4 h. The g-C_3N_4@TiO_2NRs were immobilized onto the LDPE films using a previously reported protocol [16]. In brief, the films were immersed in an aqueous suspension containing 0.4 g L^{-1} of g-C_3N_4@TiO_2NRs at an initial pH of 5.0 and subsequently irradiated for 5 h using a 200 W Xe arc lamp (Newport, USA), which had an estimated average irradiance of 3.6 mW m^{-2} nm^{-1} in the 320–430 nm range. This system was equipped with the following glass irradiation cut-off filters: UV-A + visible; cut-off filter with $\lambda > 320$ nm (Newport, USA). The UV-A emission was measured using a Lutron YK-35UV UV light meter that supplied 35 W m^{-2} (Fig. S1). After the nanorods were immobilized on the polymer surface, the films were sonicated thrice for 5 min and dried at 40 °C for 24 h. As control

material, The P25 TiO_2 nanoparticles were immobilized onto the LDPE films using a previously the same methodology as was previously reported by our research group [16].

The films were characterized by XPS, diffuse reflectance UV–Vis spectroscopy (DRS), scanning electronic microscopy (SEM) coupled with energy dispersion spectroscopy (EDS), and atomic force microscopy (AFM). All experimental details are provided in the supplementary material.

2.4. Photocatalytic activity of g-C_3N_4@TiO_2NR*/LDPE films*

2.4.1. Photobleaching experiments of the solid–liquid interface under UV and visible light irradiation

The solid–liquid interface experiments were carried out using a method based on an ISO test developed by Mills et al. [30] to evaluate photoinduced self-cleaning properties of TiO_2 films. In the present study, malachite green solution ($1x10^{-4}$ mol L^{-1}) at an initial pH of 5.0 was employed. The dyed water solution was placed in a 1 cm × 1 cm quartz cuvette. Subsequently, a 1 cm × 5 cm piece of the g-C_3N_4@TiO_2NR/LDPE film was placed in the cuvette and irradiated with the 200 W Xe arc lamp equipped with the following UV-A–visible light glass cut-off filters (Newport, USA): $\lambda > 320$ nm, $\lambda > 455$ nm, and $\lambda > 590$ nm (Fig. S2); the absorbance of malachite green at 617 nm was measured using a UV–visible Lambda 35 Perkin-Elmer spectrophotometer. Four reuse cycles were performed under irradiated light at $\lambda > 455$ nm on the g-C_3N_4@TiO_2NR/LDPE films. All experiments were carried out in triplicate. The photocatalytic activity of g-C_3N_4@TiO_2NR/LDPE was compared to that of P25/LDPE films, which were also prepared using the same protocol. Temperature oscillated between 25-35 °C during the 2 h of light irradiation

2.4.2. Photobleaching experiments of the solid–gas interface under UV and visible light irradiation

The solid–gas interface experiments were performed using a protocol reported by Pérez-Obando et al. [5] (further details in supplemental information). Light irradiation was supplied by the 200 W Xe arc lamp using cut-off filters at $\lambda > 455$ nm and $\lambda > 590$ nm. Temperature and irradiation time in these experimental conditions were around 25-30 °C and 2 h

respectively. ATR–FTIR measurements of the adsorbed malachite green dye were performed using a Perkin-Elmer FTIR spectrometer equipped with an ATR accessory. The photocatalytic activity of C_3N_4@TiO_2NR/LDPE was compared to that of the P25/LDPE films.

2.4.3. Visible-light-photoinduced wettability of g-C_3N_4@TiO_2NR/LDPE films

The contact angle was measured at room temperature using a Ramé-Hart Model 500 goniometer (USA). A drop of Milli-Q water was placed on the film surface under blue light irradiation by five Phillips TL-D 18 W blue lamps (emission spectra: 400–500 nm, UV intensity: 0.1 W m^{-2}, and intensity between 290 and 1100 nm: 60 W m^{-2}); the evolution of the droplet shape was recorded using a video camera. An image analysis software (DRO Pimage Advanced v2.2) was employed to determine the contact angle. A minimum of seven measurements were taken at different positions on the film.

3. Results and discussion

3.1. Characterization of g-C_3N_4@TiO_2NR powders

The characterization of TiO_2 before g-C_3N_4 impregnation via TEM (Fig. S3), XRD (Fig. S3), and Brunauer–Emmett–Teller (BET) surface area analysis (Table 1) confirmed the formation of nanostructures. The XRD patterns reveal broad peaks that are characteristic of H-titanate nanotubes [31], while the TEM images confirm the formation of nanostructures. Heat treatment was subsequently carried out to synthesize g-C_3N_4@TiO_2 composites; this resulted in a nanostructure rearrangement that formed nanorods of anatase-TiO_2 along with g-C_3N_4, similar to that in a previous study [20]. Consequently, a typical XRD pattern corresponding to anatase-TiO_2 is observed in the g-C_3N_4@TiO_2NR powders (Fig. 1a) at 25.3° (1 0 1), 37.8° (0 0 4), 48.1° (2 0 0), 53.9° (1 0 5), 55.1° (2 1 1), 62.9° (2 0 4), 68.9° (1 1 6), 70.1° (2 2 0), and 75.3° (2 1 5) (JCPDS card no. 21-1272) [21,22,32]; the small diffraction peaks at 27.4°can be ascribed to the rutile phase (JCPDS card no. 21-1276). Comparing with the diffractogram of synthesized pure g-C_3N_4, the peak at ~27.4° matches with the indexed peak of the (0 0 2) plane of g-C_3N_4 (JCPDS card no. 87-1526), which corresponds to the interlayer stacking of the conjugated aromatic system [21,22,33]; an overlap between this species and

the (1 0 1) plane of rutile TiO_2 can also possibly explain this, and it would be in line with a previously reported analysis [34]. The as-synthesized TiO_2 nanostructured material exhibits nanorod morphology with a length and width of 33.6 ± 7.7 and 12.1 ± 2.8 nm, respectively, as determined by TEM (Fig. 1b). The g-C_3N_4@TiO_2NR isotherm (Fig. S4) reveals a type IV profile according to the IUPAC classification, which corresponds to mesoporous materials. The textural properties of the TiO_2 nanoparticles, H-titanate nanotubes, and composites are listed in Table 2. The specific surface area of the g-C_3N_4@TiO_2NR composite is noted to be ~10 times higher than that of TiO_2 nanoparticles. However, the surface area of H-titanate nanotubes is significantly higher than that of the composite, possibly owing to the plugging of nanotube cavities during the synthesis of g-C_3N_4@TiO_2NRs.

Thermal analysis (Fig. S5) revealed a total weight loss of 3.933% and exhibited three zones. Zone I (in the region between 100-150 °C) caused probably by water removal. Zone II (between 200-400 °C) produced by urea dimerization and melamine condensation to generate g-C_3N_4 as has been already proposed by Dong et al. [35] and H-titanates shrinkage caused by -OH groups removal and forming nanorods structures [36,37]. Finally, it was identified the zone III (at T> 400 °C) which could be due to collapse of nanorods structure and sublimation of g-C_3N_4 (~600 °C) [35,37,38].

Table 2. Textural properties and atomic composition of the investigated materials.

Sample	**Surface area (m^2 g^{-1})**	**Pore volume (cm^3 g^{-1})**	**Pore diameter (nm)**	**Atomic composition (at.%)**			
				C	**Ti**	**O**	**N**
TiO_2 nanoparticles	7.28	0.0236	12.96				
H-titanate nanotubes	294.2	0.7080	9.627				
g-C_3N_4@TiO_2NR	76.28	0.4636	24.31	29.4	21.8	48.6	0.27
g-C_3N_4@TiO_2NR/LDPE				64.9	9.38	25.2	0.54
P25/LDPE				45.3	15.2	39.5	-
LDPE				95.7	-	4.2	-

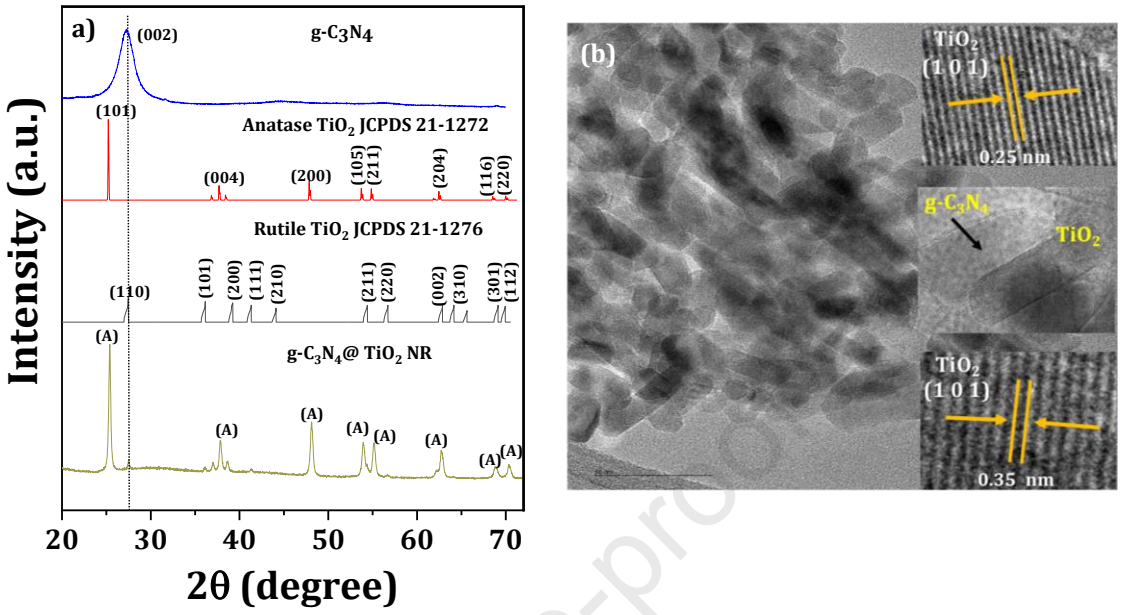

Figure 1. (a) XRD patterns of g-C_3N_4@TiO_2 NR and its comparison with rutile and anatase JCPDS charts and pure g-C_3N_4 diffractogram (b) TEM images of g-C_3N_4@TiO_2NR.

FTIR spectroscopy, UV–vis absorbance, and XPS were employed to investigate the formation of the g-C_3N_4@TiO_2NR composite. The intense IR bands between 1200 and 1600 cm^{-1} shown in Fig. 2a can be ascribed to the typical vibration modes of the heptazine heterocyclic ring units of g-C_3N_4 [23,39].

The sharp absorption band at ~1640 cm^{-1} can be assigned to the C–N stretching mode, whereas the bands at ~1250, 1330, 1400, and 1530 cm^{-1} can be attributed to the stretching vibration mode of CN heterocycles slightly shifted to longer wavelengths. These results indicate that an interaction with TiO_2 was successfully facilitated, similar to that reported in graphene/g-C_3N_4 nanocomposites [39]. Additionally, the band centered at 1540 cm^{-1} can be ascribed to N–H bending mode of unpolymerized –NH or –NH_2 on the surface or edge of g-C_3N_4.

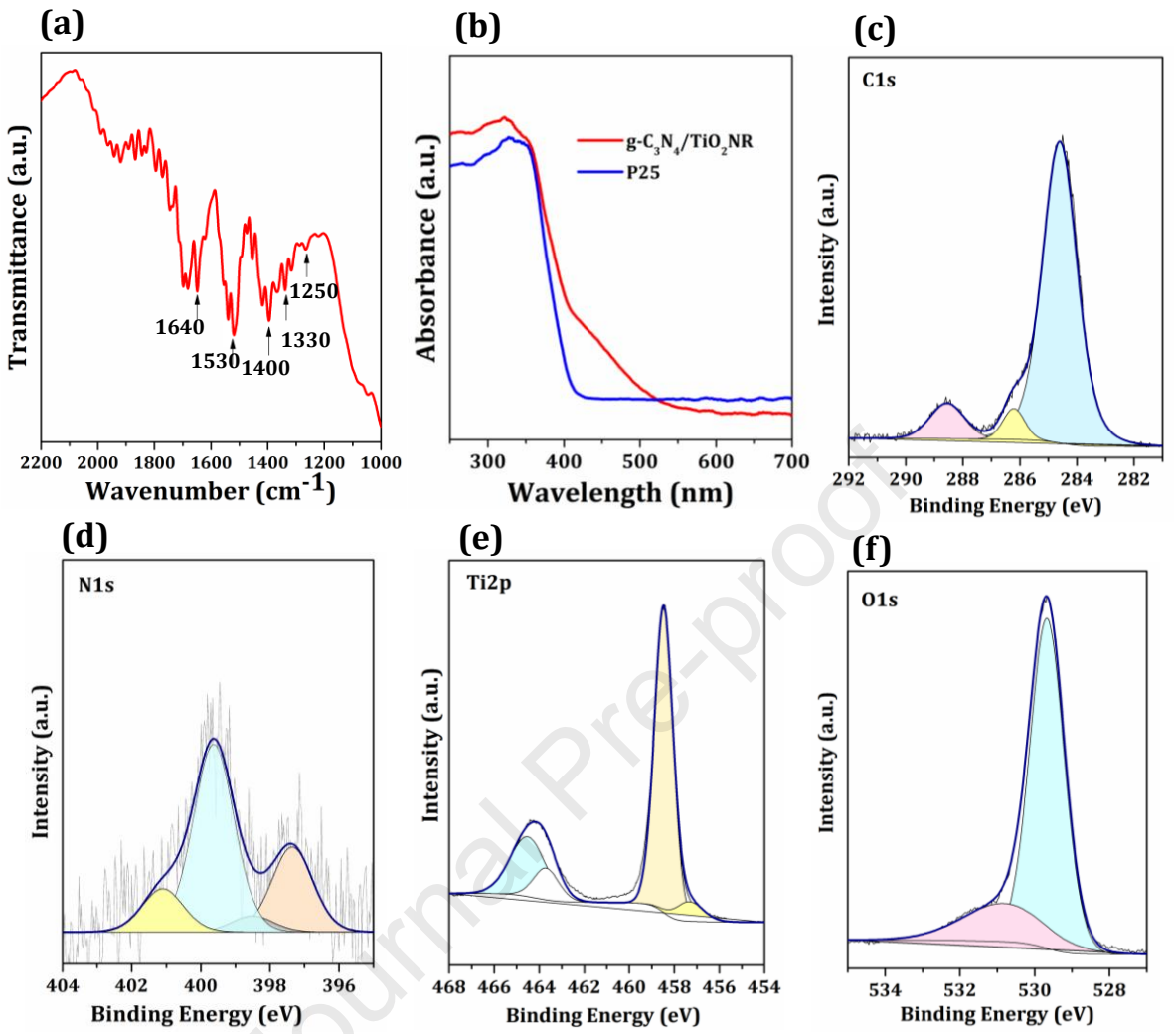

Figure 2. (a) FTIR spectra, (b) UV–vis diffuse reflectance spectra, and XPS spectra for (c) C1s, (d) N1s, (e) Ti2p, and (f) O1s core levels of g-C_3N_4@TiO_2NR.

The UV–vis diffuse reflectance spectra (Fig. 2b), on the other hand, indicate strong absorption of visible light between 400 and 500 nm for the g-C_3N_4@TiO_2 nanorods; this is possibly owing to the presence of the g-C_3N_4 species with a band gap energy of ~2.69 eV (for light absorption below 500 nm), as described previously [5,40]. TiO_2 and H-titanate nanotubes are noted to exhibit only UV light absorption.

The survey XPS spectrum of g-C_3N_4@TiO_2 nanorods shown in Fig. S6 consists of C1s, N1s, Ti2p, and O1s signals. The XPS spectra of C1s are deconvoluted into three peaks centered at 284.6, 286.3, and 288.6 eV, respectively (Fig. 2c). The first two peaks can be respectively

assigned to the C–C and C–O species from adventitious carbon, and the third peak is attributed to the sp^2-bonded carbon of the N–C=N group in g-C_3N_4, which shifts to a higher binding energy than that of pure g-C_3N_4 (288.1 eV) [41–43]. This suggests an interaction between the TiO_2NRs and g-C_3N_4; the electrons of sp^3-hybridized N atoms can navigate to the unoccupied d orbitals of Ti atoms to form a Ti–N bond. This is confirmed by the XPS peak of N1s (Fig. 2d) observed at 397.5 eV, which is assigned to Ti–N bonds [44,45] in g-C_3N_4-TiO_2 heterojunctions. The other N1s peaks detected at 398.4, 399.6, and 401.1 eV (Fig. 2d) are attributed to the sp^2-bonded N involved in the C–N=C group, tertiary nitrogen in the N–$(C)_3$ group, and free amino group in C–NH_x, respectively. It is to be noted that the observed shift to a lower binding energy of C 1s and N 1s peaks compared to that of pure g-C_3N_4 [41,46] can confirm the chemical bonding. Fig. 2e shows the high-resolution XPS spectra of Ti2p, which is deconvoluted into four peaks at 457, 458.5, 463.6, and 464.3 eV, respectively. The binding energy values at 458.5 and 464.3 eV can be assigned to the Ti $2p_{3/2}$ and Ti $2p_{1/2}$ of Ti^{4+} species; these are shifted by 0.4 eV to a lower binding energy than those measured for pristine TiO_2 [23,44,45,47]. These values also coincide with those previously reported [26,34,45] for TiO_2 modified with g-C_3N_4. Boonprakob et al. [45] explained this shift as a consequence of increased electron density on Ti via interactions between g-C_3N_4 species and TiO_2, which is supported by the XPS signal corresponding to the Ti–N bond located in the N1s region (Fig. 2d). The other two peaks centered at 457 and 463.6 eV can be attributed to Ti^{3+} species [44,48–50]. The O1s peaks in Fig. 2f at 529.7 and 531.0 eV are ascribed to O^- in TiO_2 and surface –OH groups, respectively [51]. The atomic composition of g-C_3N_4@TiO_2NR reveals the presence of C (29.36 at.%), Ti (21.81 at.%), O (48.56 at.%), and trace amounts of N (0.27 at.%) (Table 1). Therefore, the reaction of H-titanate nanotubes in the presence of urea and subsequent annealing at 450 °C were confirmed to result in the formation of visible-light-responsive g-C_3N_4@TiO_2 nanorod composites.

3.2. Characterization of g-C_3N_4@TiO_2-LDPE films

The g-C_3N_4@TiO_2 nanorod composites were photocatalytically immobilized onto the LDPE films and exhibited a strong adhesion to the polymer under ultrasonic treatment (15 min); no detachment of nanostructures was observed. Fig. 3c shows pictures of films with a

homogeneous TiO_2 layer after washing and sonication. Additionally, characterization via XPS, DRS, SEM, and AFM confirmed the TiO_2 immobilization on polymer films.

The surface chemical characterization of the g-C_3N_4@TiO_2NR/LDPE films via XPS reveals the presence of carbon (64.9 at.%), titanium (9.38 at.%), oxygen (25.2 at.%), and nitrogen (0.54 at.%) (Fig. 3a and Table 1). The Ti, O, and N results are obtained from the immobilized g-C_3N_4@TiO_2NR structures. The atomic composition results in Table 1 indicate the higher surface concentration of Ti in P25/LDPE films compared to that of the nanorod composite films.

The DRS spectrum of pristine LDPE films (black line in Fig. 3b) reveals light absorption at wavelengths below 250 nm, as discussed in a previous study [52]. However, absorption at wavelengths as high as 500 nm is also observed in photocatalytically immobilized g-C_3N_4@TiO_2NRs on LDPE films, which confirms the presence of visible-light-absorbing nanostructures. The P25/LDPE films exhibit only UV-light absorption, owing to the band gap energies of anatase and rutile TiO_2 at ~3.2 and 3.0 eV, respectively.

The SEM image (1000×) of pristine LDPE (Fig. 4a) reveals smooth surfaces, whereas that of a g-C_3N_4@TiO_2NR/LDPE film (Fig. 4b) shows dispersed micrometric aggregates probably composed of the g-C_3N_4@TiO_2 nanorods. EDS mapping and cross-sectional micrographs with Ti Kα1 and C Kα1 lines confirm the formation of a nanostructured TiO_2 layer on the LDPE surface (Fig. 4c–4f); a similarly dense TiO_2 layer is observed in the P25/LDPE films via SEM (Fig. S7).

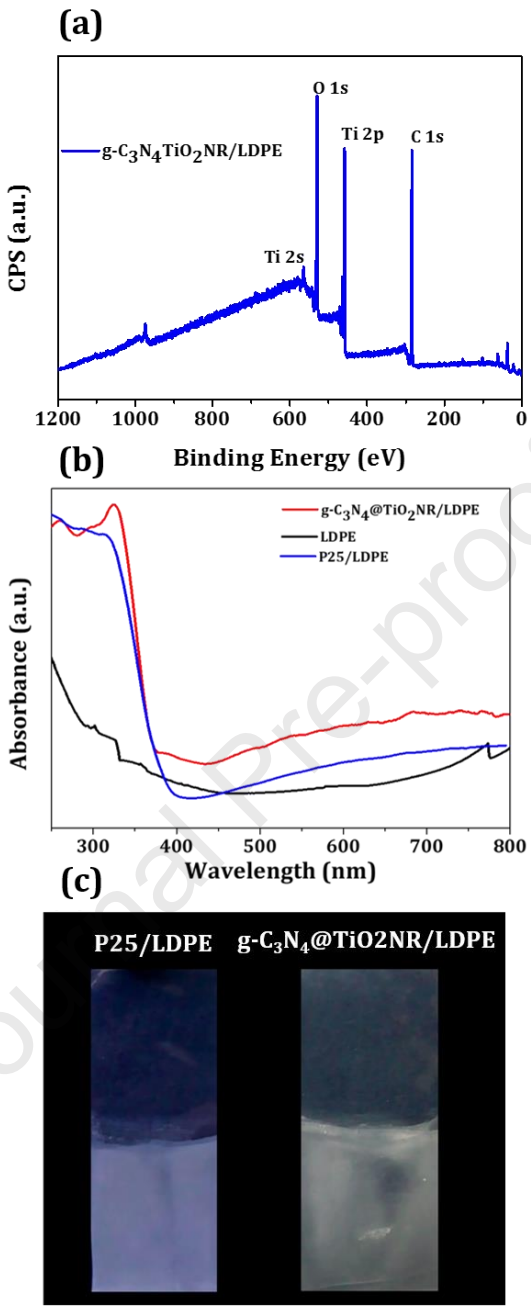

Figure 3. (a) XPS survey spectrum of g-C_3N_4@TiO_2NR/LDPE films. (b) DRS spectra and (c) pictures of C_3N_4@TiO_2NR/LDPE and P25/LDPE films after 15 min of sonication.

Fig. 5 shows AFM images obtained in a non-contact mode within a scanned area of 10 × 10 µm, which reveal the surface smoothness and low roughness (RMS = 27 nm) of the pristine LDPE film (Fig. 5a); however, the AFM images of the g-C_3N_4@TiO_2NR/LDPE films (Fig. 5b) indicate a significant increase in the roughness (RMS = 117 nm), owing to the presence

of micrometric nanorod aggregates in the g-C_3N_4@TiO_2 composites, similar to those shown in the SEM images. Moreover, the AFM images of the P25/LDPE films (Fig. S8) indicate a higher roughness (RMS) of ~305 nm owing to the higher content of TiO_2.

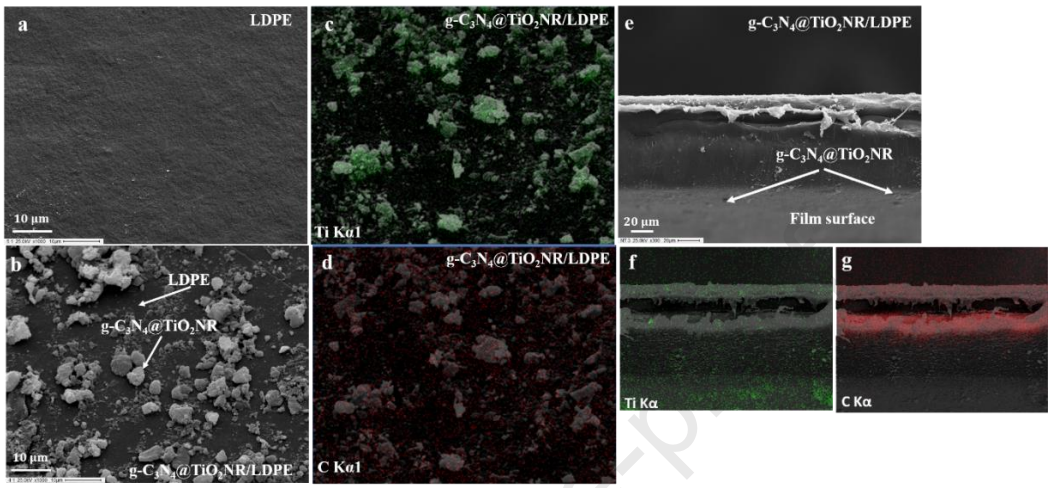

Figure 4. SEM images (1000×) of (a) LDPE and (b) C_3N_4@TiO_2NR/LDPE films. EDS mapping of C_3N_4@TiO_2NR/LDPE films with (c) Ti Kα1 and (d) C Kα1. (e) Cross-sectional SEM image of a C_3N_4@TiO_2NR/LDPE film, and EDS mapping with (f) Ti Kα1 and (g) C Kα1.

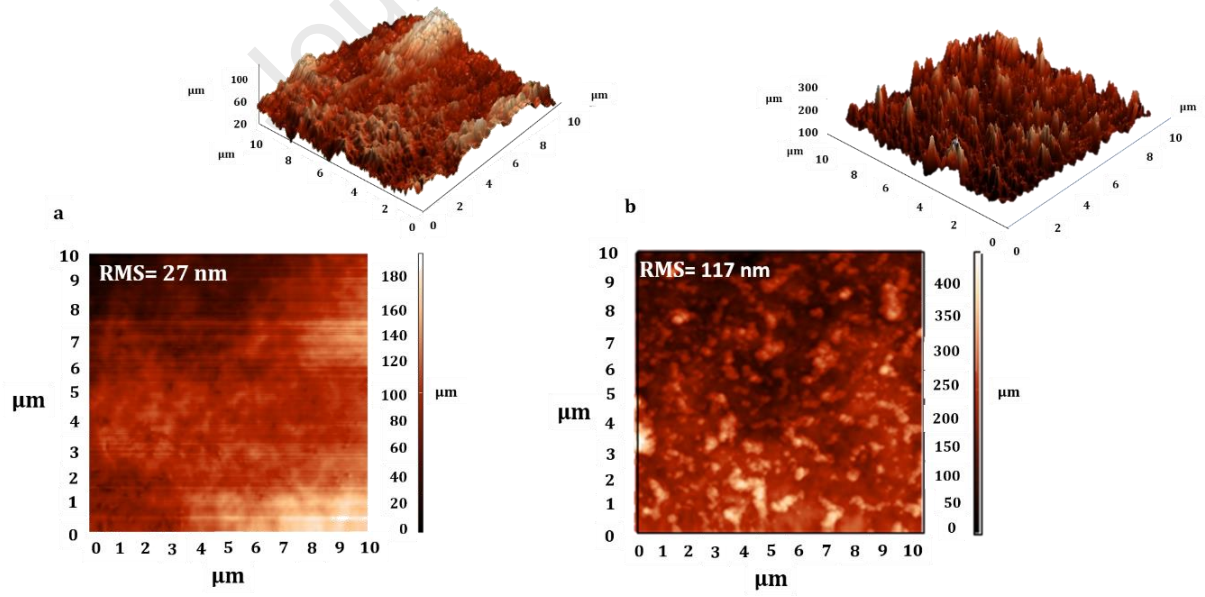

Figure 5. AFM images in non-contact mode within a scanned area of 10 × 10 µm of (a) pristine LDPE and (b) C_3N_4@TiO_2NR/LDPE films.

Overall, these results confirmed the photocatalytic immobilization of g-C_3N_4@TiO_2NRs onto LDPE films. Alvear-Daza et al. [16] demonstrated that the optimal photocatalytic immobilization of P25 nanoparticles onto LDPE films was achieved at low TiO_2 concentrations, circumneutral pH, and an irradiation time of 5 h through polymer surface functionalization induced by photogenerated •OH radicals. In the present study, Z-potential analysis (Fig. S8) was also carried out. The results indicate that the g-C_3N_4@TiO_2NR structures possess a Z-potential (pH_{pzc}) of ~6.42. At pH 5.0 (Figure S9), Z-potential exhibits a value around +0.2 mV indicating the minority existence of Ti-OH_2^+ and mainly Ti-OH groups on the surface of nanocomposites. Both surface species could interact with the photoinduced surficial oxygenated species on the LDPE films [53,54]; this further proves the immobilization of g-C_3N_4@TiO_2NRs.

3.3 Photocatalytic activity of fabricated films

3.3.1 Photocatalytic activity of g-C_3N_4@TiO_2NR/LDPE and P25/LDPE films in solid–liquid and solid–gas interfaces under UV and visible light irradiation

Fig. 6 shows the results of photobleaching of aqueous malachite green solutions by the g-C_3N_4@TiO_2NR/LDPE and P25/LDPE films under UV-A and visible light irradiation. Under irradiation at $\lambda > 320$ nm (Fig. 6a), P25/LDPE films show the highest photocatalytic activity with a color removal of approximately 90% after 2 h. In contrast, g-C_3N_4@TiO_2NR/LDPE films exhibit a color reduction ~80% at the same irradiation time. The dark adsorption of malachite green is ~20% and 17% for the g-C_3N_4@TiO_2NR/LDPE and P25/LDPE films respectively; malachite green does not undergo appreciable photolysis under this irradiation. Under visible light irradiation with $\lambda > 455$ nm (Fig. 6b), the g-C_3N_4@TiO_2NR/LDPE films exhibit the highest photobleaching activity (color removal of ~50% after 120 min), whereas that of the P25/LDPE films is ~20%. The dark experiment results reveal that the malachite green adsorption is higher in the g-C_3N_4@TiO_2NR/LDPE films compared to that in the P25/LDPE films. It is to be noted that malachite green does not undergo the photolysis reaction, and therefore, the participation of the excited states of malachite green in photobleaching reactions can be discarded. Triphenylmethane dyes, such as malachite green, are known to undergo photobleaching reactions under visible light irradiation containing

wavelengths that feature the main absorption band of the dye [55]. Non-radiative relaxation of these excited states can lead to the generation of ROS, which results in dye oxidation. Furthermore, the malachite green excited states can move electrons to the semiconductor conduction band (CB) and lead to dye degradation; this has been reported in other dyes [56,57]. Malachite green absorbs light mainly at 617 nm in aqueous solutions, and thus, visible light with $\lambda > 590$ nm was employed to perform these photochemical experiments (Fig. 6c). The results clearly indicate that photobleaching does occur because of photochemical reactions involving the malachite green excited states, which play a minor role. The dark experiment on dye adsorption on g-C_3N_4@TiO_2NR/LDPE films exhibits a trend similar to that of the photosensitized reactions, where both the light and dark experimental results ($\lambda > 590$ nm) nearly overlap.

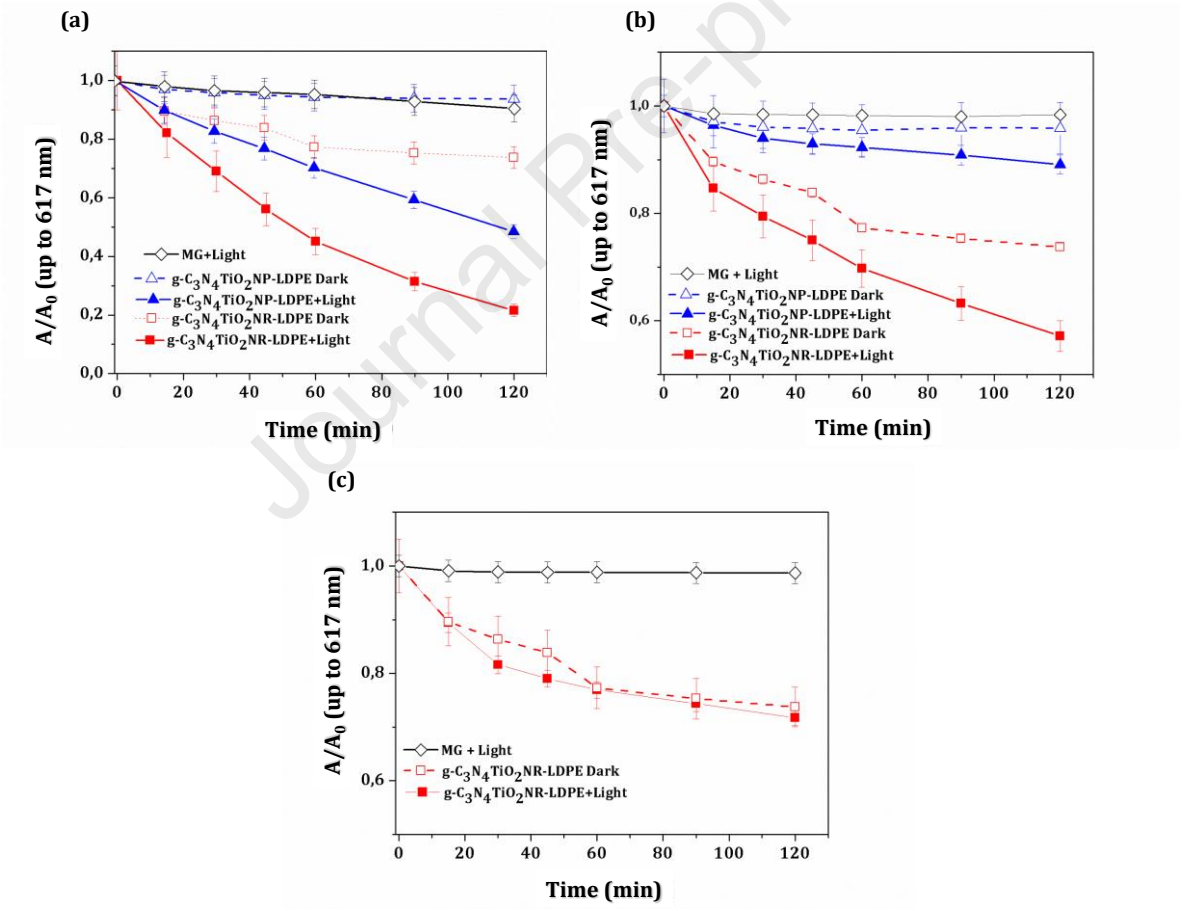

Figure 6. Solid–liquid malachite green photobleaching experiments at an initial pH of 5.0 performed with C_3N_4@TiO_2NR/LDPE and P25/LDPE films. (a) $\lambda > 320$ nm, (b) $\lambda > 455$ nm, and (c) $\lambda > 590$ nm.

The malachite green absorption spectra in experiments performed with g-C_3N_4@TiO_2NR/LDPE films (Fig. S10) at different irradiation times do not show new light-absorption bands; however, a discrete blue shift of the main absorption band of the dye is observed, which is possibly related to the N-demethylated reactions caused by the attack of photoinduced •OH radicals [58]. The results indicate that under visible light (λ > 455 nm) the g-C_3N_4@TiO_2NR/LDPE films possess a higher photocatalytic activity than that of P25/LDPE films.

The solid–liquid interface reuse experiments were performed with g-C_3N_4@TiO_2NR/LDPE films under visible light irradiation at λ > 455 nm. Four reuse cycles of 120 min each were carried out (Fig. 7).

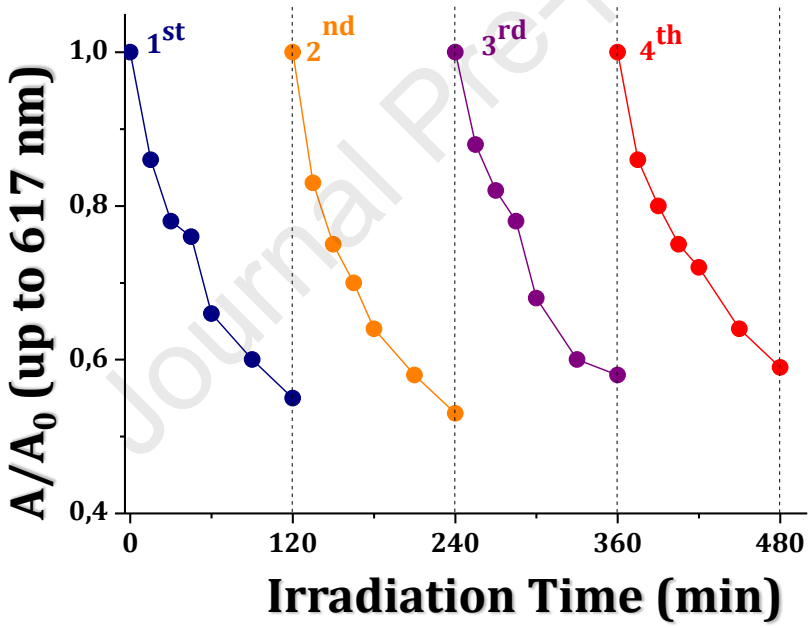

Figure 7. Solid–liquid interface reuse experiments on photobleaching of a malachite green aqueous solution at an initial pH of 5.0 performed on g-C_3N_4@TiO_2NR/LDPE films under visible light irradiation at λ > 455 nm.

The first two cycles indicate that the aqueous solution with malachite green undergoes a photobleaching of 45 and 47% respectively; the activity is noted to slightly reduce in the third and fourth cycles. Therefore, the photoinduced activity of g-C_3N_4@TiO_2NR/LDPE

films under visible light irradiation is not significantly reduced after at least four continuous cycles.

Malachite green photobleaching experiments in the solid–gas phase on g-C_3N_4@TiO_2NR/LDPE films were carried out under visible light irradiation at λ > 455 nm and λ > 590 nm (Fig. 8). The dye discoloration was tracked using color changes (pictures) and ATR–FTIR spectra obtained at each irradiation time. The dye stain is observed to be almost completely removed after 120 min of light irradiation at λ > 455 nm, whereas a comparatively minor photobleaching effect is achieved at λ > 590 nm.

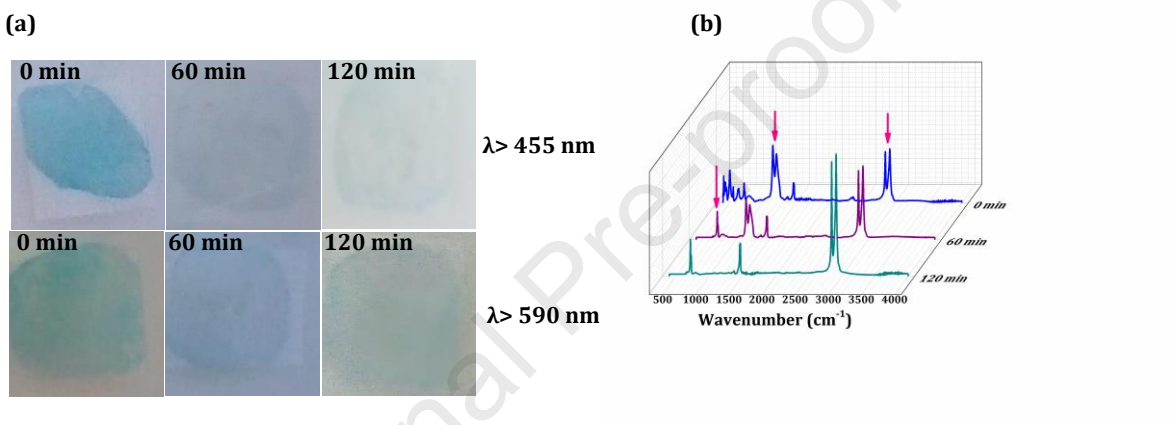

Figure 8. Solid–gas interface malachite green photobleaching experiments performed on g-C_3N_4@TiO_2NR/LDPE films under irradiated light at (a) λ > 455 nm and (b) λ > 590 nm. (c) ATR–FTIR spectra of malachite green stains on g-C_3N_4@TiO_2NR/LDPE films under λ > 455 nm irradiation.

ATR–FTIR measurements were obtained to evaluate the degradation of malachite green in the solid–gas interface on g-C_3N_4@TiO_2NR/LDPE films under light irradiation at λ > 455 nm (Fig. 8c). The peaks observed in C–H stretching (2700–3000 cm^{-1}), C–H bending vibrations (1460 cm^{-1}), and C–H out-of-plane regions (726 cm^{-1}) are all associated with LDPE (highlighted with pink arrows). The degradation of malachite green can be tracked in the bands between 1400 and 1000 cm^{-1} (highlighted with a black arrow), which correspond to the C–N stretching absorption of the dye molecule. These bands are noted to completely disappear after 120 min of visible light irradiation, with the remaining signals corresponding to the C–H vibrations of LDPE whose intensity increased at once malachite green molecules

were oxidized by photoinduced ROS. These results demonstrated that in solid/gas interfaces, visible-light photogenerated ROS in TiO_2@g-C_3N_4 composites such as $^1O_2$ and $O_2^{-\bullet}$ could participate in the chemical oxidation of malachite green molecules present on the film surface as it has already reported by Huang et al. and Pérez-Obando et al. using TiO_2@g-C_3N_4 nanocomposites immobilized on glass and chitosan in the degradation of NO_x and malachite green stains respectively. the malachite green molecules underwent photobleaching, which was probably caused by the N-demethylation reactions induced by ROS in visible-light-irradiated g-C_3N_4@TiO_2NR; this has been previously explained using the blue shift of the main absorption band of the dye. Several studies have described the photooxidation of organic dyes such as rhodamine B and methylene blue via visible-light-irradiated g-C_3N_4-TiO_2 (nanoparticles or nanorods) heterojunctions in aqueous solutions [40,59,60]. These photooxidation reactions are possibly mediated by photoinduced ROS generated on g-C_3N_4–TiO_2. Previous studies on melon/TiO_2 nanoparticles immobilized on chitosan films have indicated that these systems can photoinduce ROS such as $^{\bullet}OH$ radicals and singlet oxygen ($^1O_2$) under visible light irradiation; both are likely responsible for malachite green degradation [5].

The electronic properties of nanostructured TiO_2, crystalline phases, and features linked to film surface characteristics are known to dominate the self-cleaning activity observed in these synthesized films. Moreover, results from our previous studies have shown that the melon-TiO_2 nanoparticles immobilized on chitosan films required an irradiation time of 360 min at $\lambda > 455$ nm to photobleach malachite green stains, which was 3 times greater than that of the C_3N_4@TiO_2NR/LDPE films reported in the present study [5]. The rapid removal of malachite green stains in solid–gas interfaces using g-C_3N_4@TiO_2NR/LDPE films (120 min) clearly reveals their enhanced performance as self-cleaning surfaces than those previously reported by our group. This is possibly owing to the presence of nanostructured TiO_2.

3.3.2 Visible-light-photoinduced wettability of g-C_3N_4@TiO_2NR/LDPE films

The contact angle of water drops on pristine LDPE surfaces is known to oscillate between 102° and 106° [61] owing to its hydrophobic features. Fig. 10 reveals that commercial LDPE films possess a contact angle of ~108°, which agrees with previously reported results; this does not change even after 60 min of visible light irradiation (blue light).

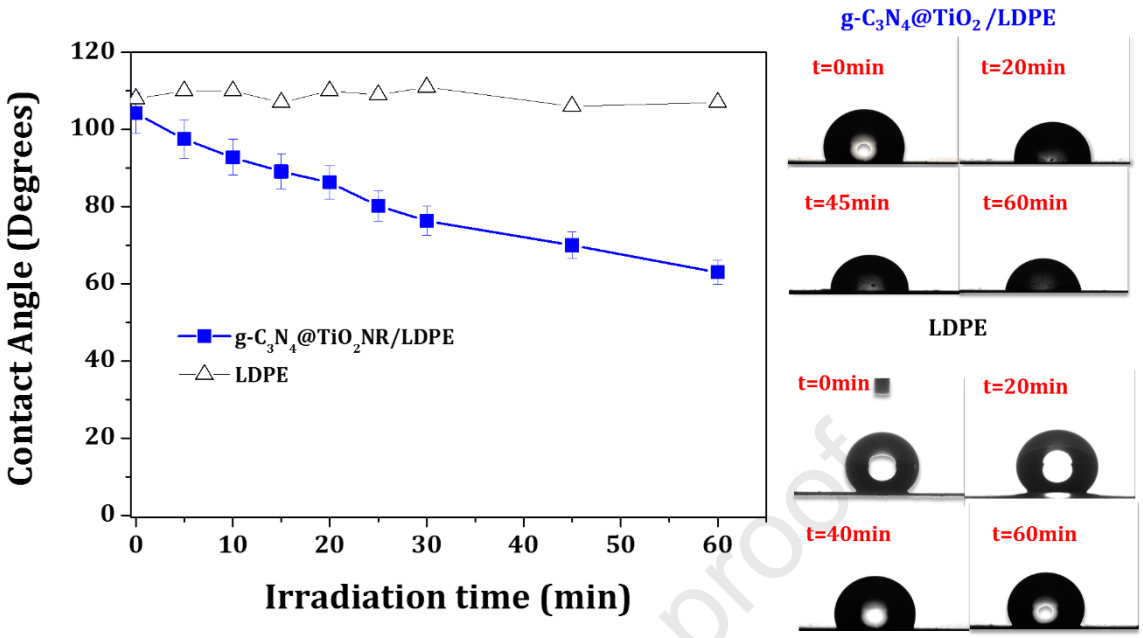

Figure 9. Wettability of LDPE and g-C_3N_4@TiO_2NR/LDPE films under blue light irradiation (400–500 nm) and a light intensity of 60 W m^{-2} in 290–1100 nm.

The contact angle in g-C_3N_4@TiO_2NR/LDPE films is observed to significantly decrease from 108° to 63° (~40%) after 60 min of blue light irradiation (Fig. 10), which demonstrates that the film becomes hydrophilic under visible light irradiation. The UV-photoinduced hydrophilicity of TiO_2 surfaces has often been linked to the formation of surficial Ti^{3+} sites via CB electrons trapped on Ti^{4+} sites, which modify the interactions between water molecules and the semiconductor surface to result in an increase in the wettability [62,63].

A few studies have reported visible-light-photoinduced hydrophilicity in TiO_2-based materials. Kwon et al. [64] claim that TiO_2 materials sensitized with organic dyes and immobilized on glass achieve a contact angle reduction of ~20%. The comparatively significant visible-light-photoinduced wettability of g-C_3N_4@TiO_2NR/LDPE films in the present study is possibly related to the increased roughness facilitated by the TiO_2 nanorods. Materials exhibiting increased roughness (and a high specific surface area) can possess a significant concentration of photoinduced Ti^{3+} sites that can enhance the wettability of these surfaces [63].

3.4. Possible photoinduced processes during MG degradation on g-C_3N_4@TiO_2NR/LDPE films

Under UV-A irradiation, P25 nanoparticles immobilized onto LDPE films exhibited improved photobleaching activity; however, when visible light irradiation was used, the films containing modified nanorods showed comparatively better photobleaching of malachite green aqueous solutions. Nanorods can offer numerous active sites and a low electron–hole recombination rate that can increase the formation of ROS. Under visible light irradiation (λ > 455 nm), the g-C_3N_4 structures are likely responsible for the light absorption (E_{bg} = 2.69 eV) by promoting electrons from its valence band (VB) to the CB to create electron–hole pairs. The CB potential of g-C_3N_4 (~ −1.3 V vs NHE at pH 7.0) facilitates electron transfer from the g-C_3N_4 CB to anatase (CB potential of −0.5 V vs NHE at pH 7.0) or rutile (CB potential of −0.3 V vs NHE at pH 7.0) TiO_2 and decreases the extent of charge carrier recombination. Using time-resolved DRS and electrochemical impedance spectroscopy, Elbanna et al. [65] and Shi et al. [66] demonstrated quick and efficient electron transfer from g-C_3N_4 to TiO_2 structures under visible light irradiation. These photoinduced electrons can be further transferred to the molecular-oxygen-generating superoxide radical ($O_2^{-\bullet}$), which undergoes disproportionation reactions in the aqueous phase that results in the formation of H_2O_2 [67]. H_2O_2 can be further reduced by photoinduced CB electrons to yield hydroxyl radicals ($^{\bullet}OH$) [68]. Additionally, the electrons transferred to the CB of rutile or anatase TiO_2 nanorods generate numerous Ti^{3+} sites that are responsible for the observed visible-light-photoinduced wettability.

A photoinduced hole in the VB of g-C_3N_4 is unlikely to yield $^{\bullet}OH$ because of its significantly negative redox potential compared to that of water oxidation [69]. However, the formation of photoinduced singlet oxygen ($^1O_2$) is facilitated via oxidation of the superoxide radical by photoinduced VB holes in g-C_3N_4 [70]. Moreover, the visible-light-photoinduced electron in the CB of g-C_3N_4 can also reduce molecular oxygen and H_2O_2 to yield superoxide and $^{\bullet}OH$ radicals, respectively (Fig. 10). This mechanism agrees well with that proposed by Boomprakob et al. [71]. Both singlet oxygen and hydroxyl radicals can oxidize malachite green molecules; the former can lead to the formation of benzophenones, whereas the latter can induce the formation of N-demethylated molecules and other byproducts [58,72], all of

which are colorless molecules. Solid–liquid self-cleaning experiments under irradiation at λ > 455 nm reveal that the main absorption band of malachite green undergoes a slight blue shift (Fig. S9) that is possibly produced via N-demethylation reactions involving an attack by •OH radicals [58].

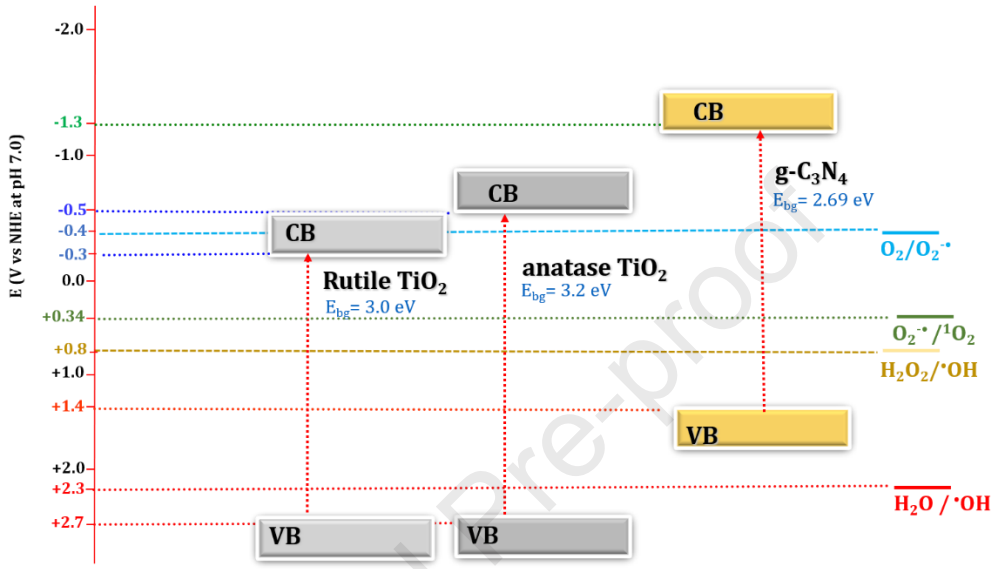

Figure 10. Scheme featuring several charge transfer-based photoinduced processes in g-C_3N_4@TiO_2 nanorods via visible light irradiation.

The textural features of P25/LDPE and g-C_3N_4@TiO_2NR/LDPE films are also possibly responsible for the observed photocatalytic activity. TiO_2 films with increased roughness are known to exhibit enhanced photoinduced activities, probably owing to their high capacities for adsorbing pollutant molecules [73]. Under visible light, the presence of visible-light-absorbing nanostructured g-C_3N_4@TiO_2 and its textural properties are likely responsible for the improved photocatalytic activity of the fabricated films, compared to those of P25/LDPE and our previously fabricated films [5].

Conclusions

Visible-light-responsive composites of g-C_3N_4@TiO_2 nanorods with polycrystalline features owing to the simultaneous presence of rutile and anatase phases were synthesized using urea as a precursor. These composites were subsequently deposited on LDPE films (denoted as g-C_3N_4@TiO_2NR/LDPE) using a new method based on photocatalytic immobilization.

Characterization of the fabricated films demonstrated the effective immobilization of g-C_3N_4@TiO_2 composites, and the films exhibited improved photocatalytic activity under visible light irradiation compared to that of P25/LDPE films. The improved visible-light-photoinduced response was likely related to the g-C_3N_4 structures that led to the generation of visible-light-photoinduced electron–hole pairs that could be transferred to the CB of rutile or anatase phases of TiO_2. The subsequent prevention of electron–hole recombination and supply of electrons that could reduce oxygen molecules yielded superoxide radicals ($O_2^{-\bullet}$) that led to the generation of $^{\bullet}OH$ and singlet oxygen ($^1O_2$); both ROS were possibly responsible for the observed photobleaching of malachite green stains. Moreover, the photoinduced charge transfer was likely responsible for the visible-light-photoinduced wettability observed on these surfaces. these fabricated films with desirable photocatalytic properties will be evaluated as potential visible-light-photoinduced antimicrobial surfaces to facilitate the abatement of bacteria and viruses via their self-cleaning properties.

Acknowledgements

The authors thank Mariela Theiller and Marcos Meyer for their experimental collaboration. Dr. Osorio-Vargas are grateful to Universidad Tecnológica de Pereira for the financial support of D. Pais-Ospina's scientific traineeship.

Funding: This work was supported by CONICET [grant PIP 0449]; Universidad Nacional de La Plata [grant X-773 and X-732]; Universidad Tecnológica de Pereira [grant 9-18-2]; CONICYT-ANID Project [FONDECYT 1191465].

References

[1] S. Rtimi, C. Pulgarin, R. Sanjines, J. Kiwi, Kinetics and mechanism for transparent polyethylene-TiO2films mediated self-cleaning leading to MB dye discoloration under sunlight irradiation, Appl. Catal. B Environ. 162 (2015) 236–244. doi:10.1016/j.apcatb.2014.05.039.

[2] L. Wu, Y. Yu, J. Zhi, Low cost and large-area fabrication of self-cleaning coating on polymeric surface based on electroless-plating-like solution deposition approach, RSC Adv. 5 (2015). doi:10.1039/c4ra10513c.

[3] A. McNeill, N. Wells, Y. Xu, X. Li, S.E.J. Bell, A. Mills, Production and testing of novel photocatalytic TiO2 surface-exposed nanoparticle (TiO2-SEN) thin plastic films, J. Photochem. Photobiol. A Chem. 369 (2019) 142–149. doi:10.1016/j.jphotochem.2018.10.025.

[4] N. Vodišek, A. Šuligoj, D. Korte, U.L. Štangar, Transparent photocatalytic thin films on flexible polymer substrates, Materials (Basel). 11 (2018). doi:10.3390/ma11101945.

[5] J. Pérez-Obando, D.A. Marín-Silva, A.N. Pinotti, L.R. Pizzio, P. Osorio-Vargas, J.A. Rengifo-Herrera, Degradation study of malachite green on chitosan films containing heterojunctions of melon/TiO2 absorbing visible-light in solid-gas interfaces, Appl. Catal. B Environ. 244 (2019) 773–785. doi:10.1016/j.apcatb.2018.12.004.

[6] E. Vélez-Peña, J. Pérez-Obando, D. Pais-Ospina, D.A. Marín-Silva, A. Pinotti, A. Cánneva, J.A. Donadelli, L. Damonte, L.R. Pizzio, P. Osorio-Vargas, J.A. Rengifo-Herrera, Self-cleaning and antimicrobial photo-induced properties under indoor lighting irradiation of chitosan films containing Melon/TiO2 composites, Appl. Surf. Sci. (2019) 144895. doi:10.1016/j.apsusc.2019.144895.

[7] D. V. Bavykin, F.C. Walsh, Elongated titanate nanostructures and their applications, Eur. J. Inorg. Chem. (2009) 977–997. doi:10.1002/ejic.200801122.

[8] T. Tachikawa, S. Tojo, M. Fujitsuka, T. Sekino, T. Majima, Photoinduced charge separation in titania nanotubes, J. Phys. Chem. B. 110 (2006) 14055–14059. doi:10.1021/jp063800q.

[9] H. Bin Wu, H.H. Hng, X.W.D. Lou, Direct synthesis of anatase TiO 2 nanowires with enhanced photocatalytic activity, Adv. Mater. 24 (2012) 2567–2571.

doi:10.1002/adma.201200564.

[10] R.P. Lynch, A. Ghicov, P. Schmuki, A Photo-Electrochemical Investigation of Self-Organized TiO[sub 2] Nanotubes, J. Electrochem. Soc. 157 (2010) G76. doi:10.1149/1.3276455.

[11] S. Abou Rich, T. Dufour, P. Leroy, F. Reniers, L. Nittler, J.J. Pireaux, LDPE surface modifications induced by atmospheric plasma torches with linear and showerhead configurations, Plasma Process. Polym. 12 (2015) 771–785. doi:10.1002/ppap.201400097.

[12] J. Fresnais, J.P. Chapel, L. Benyahia, F. Poncin-Epaillard, Plasma-treated superhydrophobic polyethylene surfaces: Fabrication, wetting and dewetting properties, J. Adhes. Sci. Technol. 23 (2009) 447–467. doi:10.1163/156856108X370127.

[13] S. Rtimi, J. Kiwi, Bactericide effects of transparent polyethylene photocatalytic films coated by oxides under visible light, Appl. Catal. B Environ. 213 (2017) 62–73. doi:10.1016/j.apcatb.2017.05.004.

[14] F. Mazille, T. Schoettl, C. Pulgarin, Synergistic effect of TiO2and iron oxide supported on fluorocarbon films. Part 1: Effect of preparation parameters on photocatalytic degradation of organic pollutant at neutral pH, Appl. Catal. B Environ. 89 (2009) 635–644. doi:10.1016/j.apcatb.2009.01.027.

[15] A.C. Mena, S. Rtimi, C. Pulgarin, J.C. Lavanchy, J. Kiwi, Grafted semiconductors on PE-films leading to bacterial inactivation: Synthesis, characterization and mechanism, Colloids Surfaces A Physicochem. Eng. Asp. 519 (2017) 231–237. doi:10.1016/j.colsurfa.2016.07.034.

[16] J. Alvear-Daza, D. Pais-Ospina, D.A. Marin-Silva, A.N. Pinotti, L. Damonte, L.R. Pizzio, P. Osorio-Vargas, J.A. Rengifo-herrera, Facile photocatalytic immobilization strategy for P-25 TiO2 nanoparticles on low density polyethylene films and their UV-A photo-induced super hydrophilicity and photocatalytic activity, (2020) In press. doi:10.1016/j.cattod.2020.07.029.

[17] L. Chi, Y. Qian, J. Guo, X. Wang, H. Arandiyan, Z. Jiang, Novel g-C3N4/TiO2/PAA/PTFE ultrafiltration membrane enabling enhanced antifouling and exceptional visible-light photocatalytic self-cleaning, Catal. Today. 335 (2019) 527–

537. doi:10.1016/j.cattod.2019.02.027.

[18] Y. Huang, P. Wang, Z. Wang, Y. Rao, J. ji Cao, S. Pu, W. Ho, S.C. Lee, Protonated g-C3N4/Ti3+ self-doped TiO2 nanocomposite films: Room-temperature preparation, hydrophilicity, and application for photocatalytic NOx removal, Appl. Catal. B Environ. 240 (2019) 122–131. doi:10.1016/j.apcatb.2018.08.078.

[19] W. Li, H. Zhang, W. Chen, L. Yang, H. Wu, N. Mao, The effects of cotton cellulose on both energy band gap of g-C3N4–TiO2 nanoparticles and enhanced photocatalytic properties of cotton-g-C3N4–TiO2 composites, Cellulose. 29 (2022) 193–212. doi:10.1007/s10570-021-04318-3.

[20] K. Hu, R. Li, C. Ye, A. Wang, W. Wei, D. Hu, R. Qiu, K. Yan, Facile synthesis of Z-scheme composite of TiO2 nanorod/g-C3N4 nanosheet efficient for photocatalytic degradation of ciprofloxacin, J. Clean. Prod. 253 (2020). doi:10.1016/j.jclepro.2020.120055.

[21] G. Li, X. Nie, J. Chen, Q. Jiang, T. An, P.K. Wong, H. Zhang, H. Zhao, H. Yamashita, Enhanced visible-light-driven photocatalytic inactivation of Escherichia coli using g-C3N4/TiO2 hybrid photocatalyst synthesized using a hydrothermal-calcination approach, Water Res. 86 (2015) 17–24. doi:10.1016/j.watres.2015.05.053.

[22] H. Bashir, X. Yi, J. Yuan, K. Yin, S. Luo, Highly ordered TiO2 nanotube arrays embedded with g-C3N4 nanorods for enhanced photocatalytic activity, J. Photochem. Photobiol. A Chem. 382 (2019) 111930. doi:10.1016/j.jphotochem.2019.111930.

[23] S. Zhou, Y. Liu, J. Li, Y. Wang, G. Jiang, Z. Zhao, D. Wang, A. Duan, J. Liu, Y. Wei, Facile in situ synthesis of graphitic carbon nitride (g-C 3 N 4) -N-TiO 2 heterojunction as an efficient photocatalyst for the selective photoreduction of CO 2 to CO, "Applied Catal. B, Environ. 158–159 (2014) 20–29. doi:10.1016/j.apcatb.2014.03.037.

[24] K. Sridharan, E. Jang, T.J. Park, Novel visible light active graphitic C3N4-TiO2 composite photocatalyst: Synergistic synthesis, growth and photocatalytic treatment of hazardous pollutants, Appl. Catal. B Environ. 142–143 (2013) 718–728. doi:10.1016/j.apcatb.2013.05.077.

[25] N. Boonprakob, N. Wetchakun, S. Phanichphant, D. Waxler, P. Sherrell, A. Nattestad, J. Chen, B. Inceesungvorn, Enhanced visible-light photocatalytic activity of g-C3N4/TiO2films, J. Colloid Interface Sci. 417 (2014) 402–409. doi:10.1016/j.jcis.2013.11.072.

[26] Z. Fu, H. Wang, Y. Wang, S. Wang, Z. Li, Q. Sun, Construction of three-dimensional g-C3N4/Gr-CNTs/TiO2 Z-scheme catalyst with enhanced photocatalytic activity, Appl. Surf. Sci. 510 (2020). doi:10.1016/j.apsusc.2020.145494.

[27] Q. Han, B. Wang, Y. Zhao, C. Hu, L. Qu, A Graphitic-C3N4 "seaweed" Architecture for Enhanced Hydrogen Evolution, Angew. Chemie - Int. Ed. 54 (2015) 11433–11437. doi:10.1002/anie.201504985.

[28] C.C. Torres, V.A. Jiménez, C.H. Campos, J.B. Alderete, R. Dinamarca, T.M. Bustamente, B. Pawelec, Gold catalysts supported on TiO2-nanotubes for the selective hydrogenation of p-substituted nitrobenzenes, Mol. Catal. 447 (2018) 21–27. doi:10.1016/j.mcat.2017.12.039.

[29] J.. Rengifo-Herrera, C. Pulgarin, Photocatalytic activity of N, S co-doped and N-doped commercial anatase TiO2 powders towards phenol oxidation and E. coli inactivation under simulated solar light irradiation, Sol. Energy. 84 (2010) 37–43. doi:10.1016/j.solener.2009.09.008.

[30] A. Mills, C. Hill, P.K.J. Robertson, Overview of the current ISO tests for photocatalytic materials, J. Photochem. Photobiol. A Chem. 237 (2012) 7–23. doi:10.1016/j.jphotochem.2012.02.024.

[31] J.N. Nian, H. Teng, Hydrothermal synthesis of single-crystalline anatase TiO2 nanorods with nanotubes as the precursor, J. Phys. Chem. B. 110 (2006) 4193–4198. doi:10.1021/jp0567321.

[32] R. Malik, V.K. Tomer, N. Joshi, T. Dankwort, L. Lin, L. Kienle, Au-TiO2-Loaded Cubic g-C3N4 Nanohybrids for Photocatalytic and Volatile Organic Amine Sensing Applications, ACS Appl. Mater. Interfaces. 10 (2018) 34087–34097. doi:10.1021/acsami.8b08091.

[33] R. Sun, X. Jiang, M. Zhang, Y. Ma, X. Jiang, Z. Liu, Y. Wang, J. Yang, M. Xie, W. Han, Dual quantum dots decorated TiO2 nanorod arrays for efficient CO2 reduction,

J. Catal. 378 (2019) 192–200. doi:10.1016/j.jcat.2019.08.035.

[34] M. Sun, Y. Fang, Y. Kong, S. Sun, Z. Yu, A. Umar, Graphitic carbon nitride (g-C3N4) coated titanium oxide nanotube arrays with enhanced photo-electrochemical performance, Dalt. Trans. 45 (2016) 12702–12709. doi:10.1039/c6dt02071b.

[35] F. Dong, M. Ou, Y. Jiang, S. Guo, Z. Wu, Efficient and durable visible light photocatalytic performance of porous carbon nitride nanosheets for air purification, Ind. Eng. Chem. Res. 53 (2014) 2318–2330. doi:10.1021/ie4038104.

[36] S. Preda, M. Rutar, P. Umek, M. Zaharescu, A study of thermal properties of sodium titanate nanotubes synthesized by microwave-assisted hydrothermal method, Mater. Res. Bull. 71 (2015) 98–105. doi:10.1016/j.materresbull.2015.07.015.

[37] A. Thorne, A. Kruth, D. Tunstall, J.T.S. Irvine, W. Zhou, Formation, structure, and stability of titanate nanotubes and their proton conductivity, J. Phys. Chem. B. 109 (2005) 5439–5444. doi:10.1021/jp047113f.

[38] W.J. Ong, L.L. Tan, Y.H. Ng, S.T. Yong, S.P. Chai, Graphitic Carbon Nitride (g-C3N4)-Based Photocatalysts for Artificial Photosynthesis and Environmental Remediation: Are We a Step Closer to Achieving Sustainability?, Chem. Rev. 116 (2016) 7159–7329. doi:10.1021/acs.chemrev.6b00075.

[39] W.J. Ong, L.L. Tan, S.P. Chai, S.T. Yong, Graphene oxide as a structure-directing agent for the two-dimensional interface engineering of sandwich-like graphene-g-C3N4 hybrid nanostructures with enhanced visible-light photoreduction of CO2 to methane, Chem. Commun. 51 (2015) 858–861. doi:10.1039/c4cc08996k.

[40] K. Sridharan, E. Jang, T.J. Park, Novel visible light active graphitic C3N4-TiO2composite photocatalyst: Synergistic synthesis, growth and photocatalytic treatment of hazardous pollutants, Appl. Catal. B Environ. 142–143 (2013) 718–728. doi:10.1016/j.apcatb.2013.05.077.

[41] G. Zhang, T. Zhang, B. Li, S. Jiang, X. Zhang, L. Hai, X. Chen, W. Wu, An ingenious strategy of preparing TiO 2 /g-C 3 N 4 heterojunction photocatalyst: In situ growth of TiO 2 nanocrystals on g-C 3 N 4 nanosheets via impregnation-calcination method, Appl. Surf. Sci. 433 (2018) 963–974. doi:10.1016/j.apsusc.2017.10.135.

[42] H.L. Meng, S.Y. Lin, J.J. Feng, L. Zhang, A.J. Wang, Coordination regulated

pyrolysis synthesis of ultrafine FeNi/(FeNi)9S8 nanoclusters/nitrogen, sulfur-codoped graphitic carbon nanosheets as efficient bifunctional oxygen electrocatalysts, J. Colloid Interface Sci. 610 (2022) 573–582. doi:10.1016/j.jcis.2021.11.101.

[43] R.M. Sun, L. Zhang, J.J. Feng, K.M. Fang, A.J. Wang, In situ produced Co9S8 nanoclusters/Co/Mn-S, N multi-doped 3D porous carbon derived from eriochrome black T as an effective bifunctional oxygen electrocatalyst for rechargeable Zn-air batteries, J. Colloid Interface Sci. 608 (2022) 2100–2110. doi:10.1016/j.jcis.2021.10.144.

[44] J. Li, M. Zhang, X. Li, Q. Li, J. Yang, Effect of the calcination temperature on the visible light photocatalytic activity of direct contact Z-scheme g-C3N4-TiO2 heterojunction, Appl. Catal. B Environ. 212 (2017) 106–114. doi:10.1016/j.apcatb.2017.04.061.

[45] N. Boonprakob, N. Wetchakun, S. Phanichphant, D. Waxler, P. Sherrell, A. Nattestad, J. Chen, B. Inceesungvorn, Enhanced visible-light photocatalytic activity of g-C3N4/TiO2 films, J. Colloid Interface Sci. 417 (2014) 402–409. doi:10.1016/j.jcis.2013.11.072.

[46] G. Zhang, J. Zhang, M. Zhang, X. Wang, Polycondensation of thiourea into carbon nitride semiconductors as visible light photocatalysts, J. Mater. Chem. 22 (2012) 8083–8091. doi:10.1039/c2jm00097k.

[47] L. Xiao, T. Liu, M. Zhang, Q. Li, J. Yang, Interfacial Construction of Zero-Dimensional/One-Dimensional g-C 3 N 4 Nanoparticles/TiO 2 Nanotube Arrays with Z-Scheme Heterostructure for Improved Photoelectrochemical Water Splitting, ACS Sustain. Chem. Eng. 7 (2019) 2483–2491. doi:10.1021/acssuschemeng.8b05392.

[48] M. Sun, S. Shen, Z. Wu, Z. Tang, J. Shen, J. Yang, Rice spike-like g-C3N4/TiO2 heterojunctions with tight-binding interface by using sodium titanate ultralong nanotube as precursor and template, Ceram. Int. 44 (2018) 8125–8132. doi:10.1016/j.ceramint.2018.01.257.

[49] Y. Fu, H. Du, S. Zhang, W. Huang, XPS characterization of surface and interfacial structure of sputtered TiNi films on Si substrate, Mater. Sci. Eng. A. 403 (2005) 25–

31. doi:10.1016/j.msea.2005.04.036.

[50] F. Qi, W. An, H. Wang, J. Hu, H. Guo, L. Liu, W. Cui, Combing oxygen vacancies on TiO2 nanorod arrays with g-C3N4 nanosheets for enhancing photoelectrochemical degradation of phenol, Mater. Sci. Semicond. Process. 109 (2020) 104954. doi:10.1016/j.mssp.2020.104954.

[51] A. Wiatrowski, M. Mazur, A. Obstarczyk, D. Wojcieszak, D. Kaczmarek, J. Morgiel, D. Gibson, Comparison of the physicochemical properties of TiO2 thin films obtained by magnetron sputtering with continuous and pulsed gas flow, Coatings. 8 (2018). doi:10.3390/COATINGS8110412.

[52] S.S. Ali, I.A. Qazi, M. Arshad, Z. Khan, T.C. Voice, C.T. Mehmood, Photocatalytic degradation of low density polyethylene (LDPE) films using titania nanotubes, Environ. Nanotechnology, Monit. Manag. 5 (2016) 44–53. doi:10.1016/j.enmm.2016.01.001.

[53] R.T. Thomas, N. Sandhyarani, Enhancement in the photocatalytic degradation of low density polyethylene-TiO2 nanocomposite films under solar irradiation, RSC Adv. 3 (2013) 14080–14087. doi:10.1039/c3ra42226g.

[54] R.T. Thomas, V. Nair, N. Sandhyarani, TiO2 nanoparticle assisted solid phase photocatalytic degradation of polythene film: A mechanistic investigation, Colloids Surfaces A Physicochem. Eng. Asp. 422 (2013) 1–9. doi:10.1016/j.colsurfa.2013.01.017.

[55] D.F. Duxbury, The Photochemistry and Photophysics of Triphenylmethane Dyes In Solid and Liquid Media, Chem. Rev. 93 (1993) 381–433.

[56] J. Zhao, C. Chen, W. Ma, Photocatalytic Degradation of Organic Pollutants Under Visible Light Irradiation, Top. Catal. 35 (2005) 269–278. doi:10.1007/s11244-005-3834-0.

[57] G. Ramakrishna, H.N. Ghosh, A.K. Singh, D.K. Palit, J.P. Mittal, Dynamics of back-electron transfer processes of strongly coupled triphenyl methane dyes adsorbed on TiO2nanoparticle surface as studied by fast and ultrafast visible spectroscopy, J. Phys. Chem. B. 105 (2001) 12786–12796. doi:10.1021/jp011078k.

[58] J.A. Rengifo-Herrera, L.R. Pizzio, M.N. Blanco, C. Roussel, C. Pulgarin, Photocatalytic discoloration of aqueous malachite green solutions by UV-illuminated

TiO2 nanoparticles under air and nitrogen atmospheres : effects of counter-ions and pH, Photochem. Photobiol. Sci. 10 (2011) 29–34. doi:10.1039/c0pp00196a.

[59] X. Wu, S. Fang, Y. Zheng, J. Sun, K. Lv, J.C. Yu, W.K. Ho, Thiourea-modified TiO2 nanorods with enhanced photocatalytic activity, Molecules. 21 (2016). doi:10.3390/molecules21020181.

[60] H. Lin, L. Zhao, Novel g-C3N4/TiO2 nanorods with enhanced photocatalytic activity for water treatment and H2 production, J. Mater. Sci. Mater. Electron. 30 (2019) 18191–18199. doi:10.1007/s10854-019-02173-4.

[61] B. Suresh, S. Maruthamuthu, M. Kannan, A. Chandramohan, Mechanical and surface properties of low-density polyethylene film modified by photo-oxidation, Polym. J. 43 (2011) 398–406. doi:10.1038/pj.2010.147.

[62] R. Wang, K. Hashimoto, A. Fujishima, M. Chikuni, E. Kojima, A. Kitamura, M. Shimohigoshi, T. Watanabe, Photogeneration of highly amphiphilic TiO2 surfaces, Adv. Mater. 10 (1998) 135–138. doi:10.1002/(SICI)1521-4095(199801)10:2<135::AID-ADMA135>3.0.CO;2-M.

[63] S. Banerjee, D.D. Dionysiou, S.C. Pillai, Self-cleaning applications of TiO2 by photo-induced hydrophilicity and photocatalysis, Appl. Catal. B Environ. 176–177 (2015) 396–428. doi:10.1016/j.apcatb.2015.03.058.

[64] G. Kwon, D. Panchanathan, S.R. Mahmoudi, M.A. Gondal, G.H. McKinley, K.K. Varanasi, Visible light guided manipulation of liquid wettability on photoresponsive surfaces, Nat. Commun. 8 (2017). doi:10.1038/ncomms14968.

[65] O. Elbanna, M. Fujitsuka, T. Majima, g-C3N4/TiO2 Mesocrystals Composite for H2 Evolution under Visible-Light Irradiation and Its Charge Carrier Dynamics, ACS Appl. Mater. Interfaces. 9 (2017) 34844–34854. doi:10.1021/acsami.7b08548.

[66] X. Shi, M. Fujitsuka, Z. Lou, P. Zhang, T. Majima, In situ nitrogen-doped hollow-TiO2/g-C3N4 composite photocatalysts with efficient charge separation boosting water reduction under visible light, J. Mater. Chem. A. 5 (2017) 9671–9681. doi:10.1039/c7ta01888f.

[67] T. Sawyer, S. Valentine, How Super Is Superoxide?, Acc. Chem. Res. (1981) 393–400. doi:10.1021/ar00072a005.

[68] K. Sahel, L. Elsellami, I. Mirali, F. Dappozze, M. Bouhent, C. Guillard, Hydrogen

peroxide and photocatalysis, Appl. Catal. B Environ. 188 (2016) 106–112. doi:10.1016/j.apcatb.2015.12.044.

[69] J. Wen, J. Xie, X. Chen, X. Li, A review on g-C 3 N 4 -based photocatalysts, Appl. Surf. Sci. 391 (2017) 72–123. doi:10.1016/j.apsusc.2016.07.030.

[70] T. Daimon, T. Hirakawa, M. Kitazawa, J. Suetake, Y. Nosaka, Formation of singlet molecular oxygen associated with the formation of superoxide radicals in aqueous suspensions of TiO 2 photocatalysts, Appl. Catal. A Gen. 340 (2008) 169–175. doi:10.1016/j.apcata.2008.02.012.

[71] N. Boonprakob, N. Wetchakun, S. Phanichphant, D. Waxler, P. Sherrell, A. Nattestad, J. Chen, B. Inceesungvorn, Enhanced visible-light photocatalytic activity of g-C3N4/TiO2 films, J. Colloid Interface Sci. 417 (2014) 402–409. doi:10.1016/j.jcis.2013.11.072.

[72] C.C. Chen, C.S. Lu, Y.C. Chung, J.L. Jan, UV light induced photodegradation of malachite green on TiO2 nanoparticles., J. Hazard. Mater. 141 (2007) 520–8. doi:10.1016/j.jhazmat.2006.07.011.

[73] X. Sun, P. Chen, M. Mujahid, L. Zhou, Effect of withdrawal speed on the microstructure, optical, and self-cleaning properties of TiO2 thin films, J. Sol-Gel Sci. Technol. 93 (2020) 62–69. doi:10.1007/s10971-019-05171-4.

- Visible-light active g-C_3N_4@TiO_2 nanorod were photocatalytically immobilized on LDPE.
- g-C_3N_4@TiO_2NR/LDPE films exhibited enhanced visible-light photocatalytic activity.
- Visible-light-photoinduced wettability was observed in g-C_3N_4@TiO_2NR/LDPE films.
- Films exhibited high visible-light photocatalytic activity after four reuse cycles.

Declaration of interests

☒ The authors declare that they have no known competing financial interests or personal relationships that could have appeared to influence the work reported in this paper.

☐The authors declare the following financial interests/personal relationships which may be considered as potential competing interests: